IEEE Robotics and Automation Letters (RAL) paper presented at the
2020 IEEE International Conference on Robotics and Automation (ICRA)
31 May - 31 August, 2020. Paris, France

Sim-to-real Transfer Learning Approach for Tracking Multi-DOF Ankle Motions Using Soft Strain Sensors

Hyunkyu Park, Junhwi Cho, Junghoon Park, Youngjin Na, Jung Kim, Member, IEEE

***Abstract*— A data-driven approach has recently been investigated for identifying human joint angles by means of soft strain sensors because of the corresponding modeling difficulty. However, this approach commonly incurs a high computational burden due to the voluminous amount of data required and the time-series-oriented network architecture. Moreover, the nature of soft sensors makes the problem worse due to the inherent nonlinearity and hysteresis of the material. In this study, we developed a novel wearable sensing brace design for measuring multiple degrees of freedom (DOF) ankle motions to minimize hysteresis and to improve the measurement repeatability and developed a computationally efficient calibration method based on sim-to-real transfer learning. By attaching the soft sensors to shin links rather than directly to the ankle joint, the effects of external disturbances during joint motions were minimized. To calibrate the sensors to body motions, transfer learning was used based on the results from musculoskeletal simulation(OpenSim) and sensor data. The average tracking error for ankle motions using the proposed method was found to be 12.0° for five healthy subjects, while the direct deep neural network approach showed an error of 17.9°. The proposed method could be used to calibrate the soft sensors with 1000 times faster training speed while maintaining comparable tracking accuracy with a smaller amount of data.**

I. Introduction

Motion tracking has been widely used in various applications in fields such as robotics, biomechanics, daily life assistance, and graphic animation [1], [2]. Various methods have been introduced for measuring body motions, such as motion capture cameras, stereoscopic cameras, and inertial measurement units (IMUs) [3]–[6]. Recently, soft strain sensors have been attracting wide attention because of the beneficial role in compliant, comfortable, and easy-to-use wearable robotics for daily life [7]. Soft strain sensors are highly stretchable, allowing for easy attachment and high compliance with joint motion. Thus, such sensors enable the estimation of human body motions by means of soft, space-unconstrained, portable and wearable devices [8]–[10]. Among the various types of soft strain sensors available, piezoresistive-type sensors [11]–[13] and capacitive-type sensors [14], [15] have both been widely utilized in wearable applications due to their simple read-out systems, easy manufacturing process, and high stretchability [9].

* This work was supported by the National Research Foundation of Korea grant funded by the Korea government under Grant NRF-2018R1A2A2A05021472. (Corresponding authors: Jung Kim; Youngjin Na)

H. Park, J. Cho, J. Park and J. Kim are with the Department of Mechanical Engineering at KAIST, Daejeon, 34141, Republic of Korea (e-mail: hkpark93; wnsgnl549; junghoon.park; jungkim@kaist.ac.kr).

Y. Na is with the Department of Mechanical Systems Engineering at Sookmyung Women's University, Seoul, 04310, Republic of Korea (e-mail: yjna@sookmyung.ac.kr).

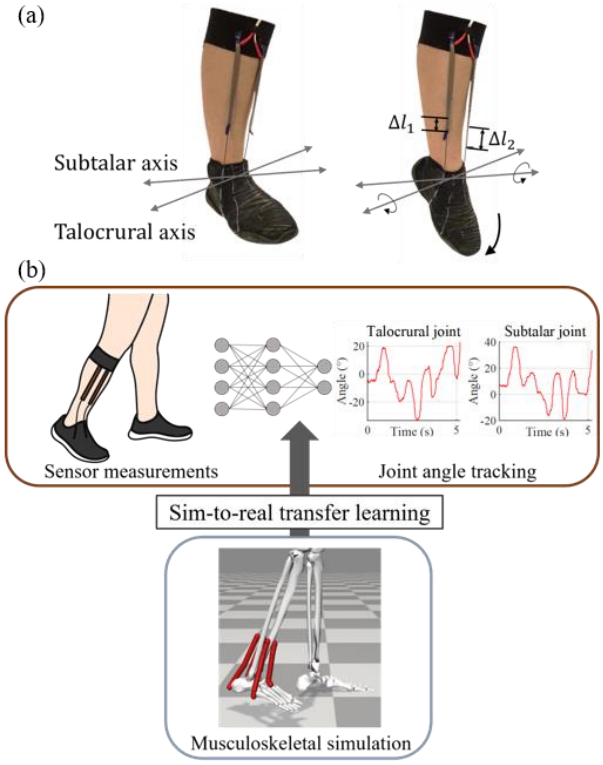

Fig. 1: Proposed wearable sensing brace for measuring multi-DOF ankle motions: (a) four soft sensors on a flexible shoe with axes of rotation at the ankle; (b) calibration process based on transfer learning and simulation.

However, several critical issues also arise in the use of soft strain sensors, namely, high nonlinearity, hysteresis and low repeatability, all of which contribute to low measurement performance [9]. These intrinsic behaviors originate from two sources: the characteristics of the sensors themselves and the effects of joint motion. The viscoelasticity of the soft materials results in time-varying and unrepeatable operation [16], [17]. In addition, joint movements cause a variety of unwanted disturbances, such as twisting and bending [8]. To address the issue of unwanted joint behavior, various methods of modifying the sensor attachment design has been proposed [8], [18]. Various numerical calibration methods have also been reported for realizing human motion tracking using soft strain sensors [8], [19]–[23]. While the numerical calibration models exhibit moderate performance, the advanced construction considering the complex behavior of soft strain sensors is required to obtain more accurate joint angle measurements.

Recently, machine learning has been used to compensate for the nonlinearity and hysteresis of soft sensors [24]–[26]. Kim et al. reported the Deep Full-Body Motion Network (DFM-Net) model for tracking whole-body poses with strain sensors [7]. A data-driven approach was adopted to construct an end-to-end mapping of the sensor signals to the user body poses measured by a motion capture camera, using a long-short-term memory (LSTM) network to accommodate the time-varying behavior of the soft strain sensors. Moreover, semi supervised learning have been reported for reducing the effort on dataset collection [18]. A support vector regression method has been utilized to achieve high-precision and well-generalizable performance for walking poses [27]. However, when measuring the various body poses that can occur in daily life, a large amount of motion data will inevitably be collected, which will lead to a trade-off between generalized measurement performance and fast and computationally efficient calibration.

In this work, we introduce a sim-to-real transfer learning approach for data-driven calibration for the tracking of multi-DOF ankle joint motion using a wearable sensing brace, as shown in Fig. 1. Sim-to-real transfer learning has been widely utilized to overcome the difficulty of dataset collection [28]. We use the OpenSim musculoskeletal simulation [29] to simulate multi-DOF joint motions at the ankle, which are then used to train the calibration model in advance. Subsequently, we fine-tune the pretrained model with individual motion data. Based on this process, the proposed calibration method can be completed with a smaller amount of data and within a remarkably short time.

We have developed a wearable sensing brace design to reduce the time-varying behavior of soft strain sensors, as shown in Fig. 1(a). The sensing brace includes four fabric-based capacitive strain sensors, which are characterized by high linearity and repeatability. The soft sensors are attached with hook-and-loop fasteners (Velcro™) to the shin link rather than being directly attached to the ankle joint. This sensing brace design was quantitatively proven to result in improved hysteresis and repeatability in the sensor operation. Based on this achievement, we can utilize a simple fully connected neural network architecture instead of a time-series-oriented architecture for calibration. The performance of the transfer-learning-based calibration method for monitoring ankle motions is verified through quantitative comparisons with direct end-to-end deep neural network (DNN)-based calibration in terms of measurement accuracy, generalized measurement capability, and the training time based on tests involving multiple users. To show the applicability of the proposed design in real-life activities, various tasks related to ankle motion are demonstrated.

II. Wearable Sensing Brace

We focused on reducing the time-varying behavior of the wearable sensing brace to enable fast and computationally efficient calibration. We selected capacitive strain sensors to meet the requirements of high linearity and repeatability and developed a sensing brace design suitable for measuring multi-DOF ankle joint motion with low hysteresis.

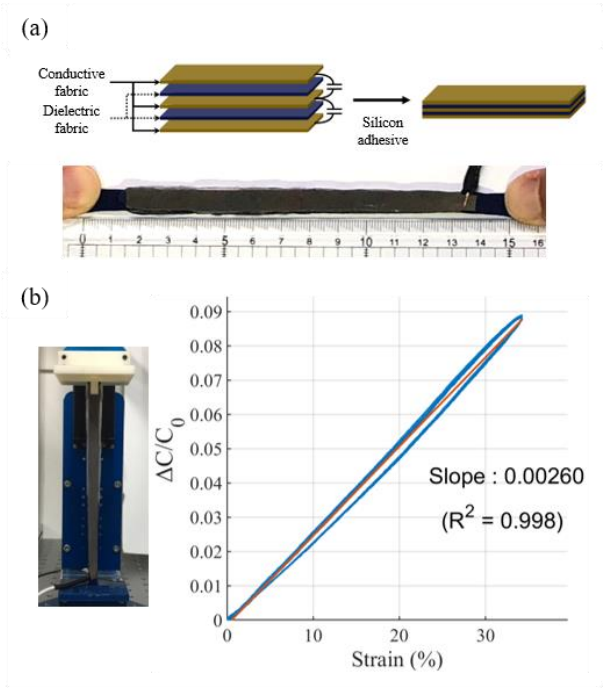

Fig. 2: Specifications of the soft strain sensors: (a) structure and schematic of a strain sensor; (b) strain-versus-capacitance characterization of a soft sensor.

A. Fabric-Based Capacitive Strain Sensors

Capacitive strain sensors have high linearity, good repeatability, and low hysteresis [14], [20], [30]. Minimizing time-varying property in sensor behavior can guarantee reliable long-term use and linearity enables the measurement of changes in length independently of the initial length of the sensor, making less dependent on users' unique physical characteristics.

The basic principle of a capacitive strain sensor is that it measures the changes in capacitance caused by changes in the distance between two pieces of conductive fabric when stretched. The sensors used in this study are designed with a five-layer structure in which conductive fabric and nonconductive polyester fabric are sequentially stacked, with final dimensions of 9.5×120×2.7 mm, as shown in Fig. 2(a) [14], [20]. The conductive layer in the middle is connected to a signal line, and the two outermost layers are grounded. The fabric layers are glued together with silicone rubber (Ecoflex™ 00-30, Smooth-On, USA). The electrode in each layer is formed by the simple attachment of a small clamp terminal. The data from all four strain sensors of the brace are simultaneously collected at a 250 Hz sampling rate using a capacitance-to-digital converter (FDC2214, Texas Instruments ™, USA).

B. Cyclic Loading Test

A cyclic loading test was conducted to investigate the mechanical properties of the sensors, as shown in Fig. 2(b). A sensor was stretched with a sinusoidal wave profile at a frequency of 0.1 Hz. Pretension was imposed by means of an initial extension length of 20 mm; the maximum extension length was 50 mm, representing the full range of changes in length that can be caused by ankle movements. The sensor

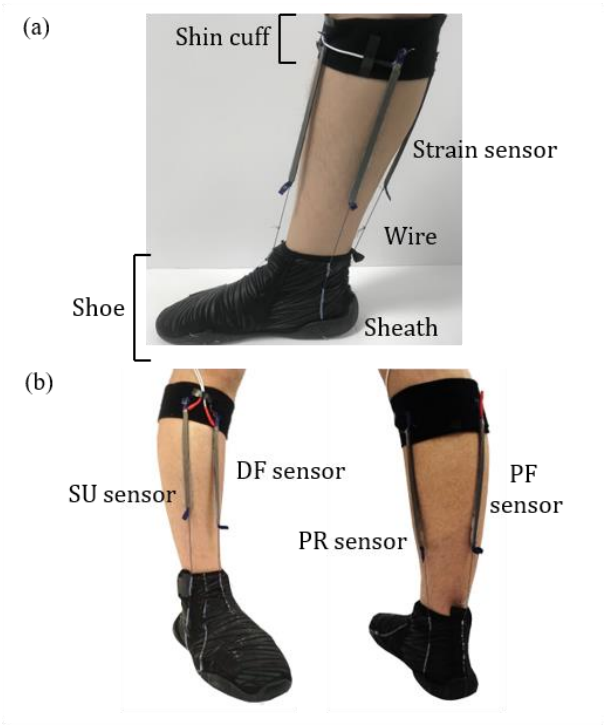

Fig. 3: Design and performance of the sensing brace: (a) overview of the proposed sensing brace; (b) names and placements of the four sensors [DF, dorsiflexion; PF, plantar flexion; PR, pronation; SU, supination].

was subjected to 500 load cycles to validate its repeatability during long-term use. Fig. 2(b) shows that the soft sensors exhibit sufficiently high linearity and repeatability with low hysteresis, as reported in previous studies [14], [20]. The results of linear regression show high linearity (R^2= 0.998), high repeatability, and a low hysteresis error (5.16%). The slope in linear fitting was used for the calibration model in this study.

C. *Sensing Brace Design*

The design of the proposed sensing brace is based on the concept of placing each sensor on a body link (shin), instead of directly attaching it to the ankle joint, and using a wire to stretch each sensor as the joint rotates. As a result, the sensors are not subjected to any unwanted deformations other than stretching by intentional joint motion. The concept of attachment to a body link was inspired by a previous report [8], and we extended this concept to multi-DOF joint movements. The sensing brace consists of four soft strain sensors, a flexible shoe with wires routed through sheaths, and a hook-and-loop fastener (Velcro™) cuff on the shin, as shown in Fig. 3(a). We selected the locations of the sensors based on the axes of rotation at the ankle [31]. The sensors for the talocrural joint axis are called the dorsiflexion (DF) and plantar flexion (PF) sensors, and the sensors for the subtalar joint axis are called the supination (SU) and pronation (PR) sensors; these sensors are arranged as shown in Fig. 3(b). The modularization of the sensing brace with the shoe and shin cuff improves user wearability and facilitates size adjustment. The shin cuff fixes one end of each sensor, and the shoe supports the wires and predetermines their paths.

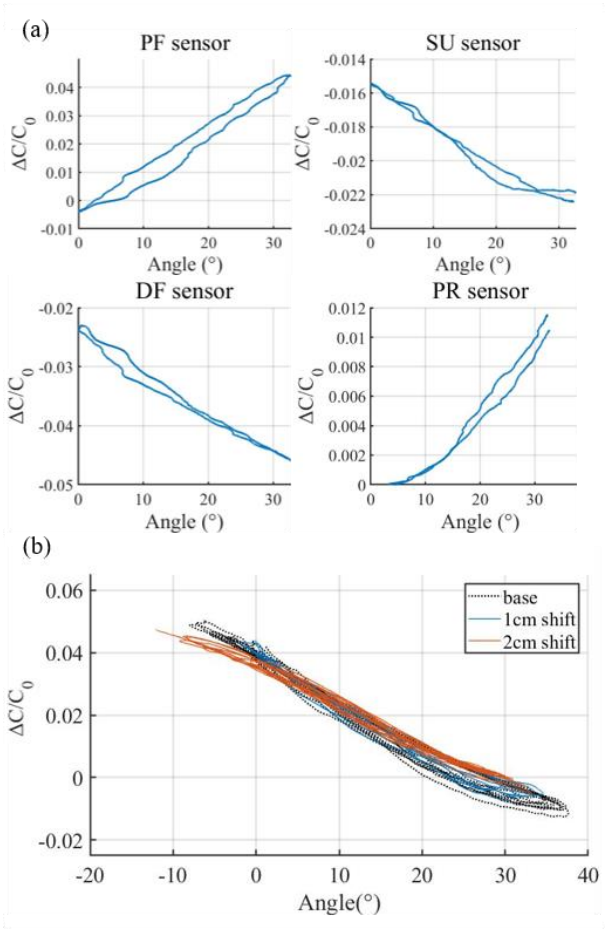

Fig. 4: Quantitative performance validation of the sensing brace design: (a) hysteresis analysis based on data collected from the four sensors during dorsiflexion and plantar flexion movements; (b) repeatability and insensitivity to sensor placement when the sensor is attached at locations higher than the baseline location by 1 cm and 2 cm.

D. *Performance Validation of the Proposed Sensing Brace*

The quantitative performance of the proposed sensing brace design was validated by measuring its hysteresis and repeatability. For the low-hysteresis performance of the sensing brace, we examined the sensor signals during dorsiflexion and plantar flexion movements, as shown in Fig. 4(a). The joint angles were measured through a motion capture experiment. The results show that the proposed brace design exhibits low hysteresis. The hysteresis errors of each sensor were measured to be 14.6% for the PF sensor, 8.63% for the SU sensor, 4.16% for the DF sensor, and 5.93% for the PR sensor.

In addition to low hysteresis, our sensing brace shows high repeatability and robustness with respect to the initial sensor location. We examined the signal from the DF sensor during 5~10 repeated dorsiflexion/plantar flexion movements while perturbing the placement of the sensor. From the initial sensor location, we stretched the sensor farther and attached it at locations that were 1 cm and 2 cm higher than its original location. The results show that the proposed sensing design enables highly repeatable operation regardless of the precise location of sensor attachment as shown in Fig. 4(b). The

slopes obtained through linear regression are -0.00140, -0.00141 and -0.00128 for the baseline location, 1 cm extension and 2 cm extension, respectively, and the corresponding coefficients of determination (R^2) are 0.990, 0.988 and 0.995. The high repeatability and insensitivity to sensor placement compared to the case of direct attachment at the joint are presumed to be due to the fact that the change in length caused by joint rotation is always fully converted into deformation of the sensors by means of wires, regardless of the sensor placement. This finding suggests that the proposed hardware design may offer reliable measurement performance even with repeated donning/ doffing of the sensing brace.

III. Transfer-Learning-Based Calibration

The calibration of a sensing device refers to tuning the sensor signal to correspond to actual movements. In this work, our aim is to monitor the angles of the two fundamental rotational axes of the ankle joint: the talocrural joint axis and the subtalar joint axis [31]. We assert that a motion representation with respect to these 2-DOF biomechanical joint axes, instead of a representation in terms of arbitrary 3-DOF Euler angles, can provide more realistic information about user activity. Here, we introduce a transfer-learning-based calibration approach to achieve fast and computationally efficient model construction. The process of sim-to-real transfer learning consists of first pretraining a calibration model on a musculoskeletal simulation dataset and then fine-tuning the model using a dataset from a motion capture experiment. We designed a multistep neural network. For comparison, we also constructed a direct end-to-end DNN with a network architecture analogous to that of the proposed transfer-learning-based model.

A. Dataset Generation in a Motion Capture Experiment

We conducted a motion capture experiment to measure the joint motions corresponding to changes in sensor signals. Six markers were attached to the foot and the links, as shown in Fig. 5(a). The motion capture device (Trio:V120, OptiTrack, USA) measured data at a sampling rate of 120 Hz. Each subject was asked to sit on a chair and move his or her foot while wearing the sensing brace during two motion sessions.

The first session involved reciprocating rotation in six directions while maintaining a neutral pose. The experimental protocol was designed to measure the angles across the entire range of motion (ROM) of each representative joint axis and to include the interdependency of the joint axes. The second session involved random circular rotation. The details of the motions performed in the two sessions are illustrated in Fig. 5(b). Both sessions for all participants were conducted without guidance feedback in order to measure the free movement of each individual. We recruited five healthy subjects (males with an average age of 21.1) to perform the requested ankle movements while wearing the developed system. All experiments were conducted with approval from the internal institutional review board of the Korea Advanced Institute of Science and Technology.

B. Musculoskeletal Simulations

Musculoskeletal simulations were performed to measure the changes in surface length (Δl) corresponding to various joint movements ($\Delta\theta_{sim}$). For this simulation, we used the

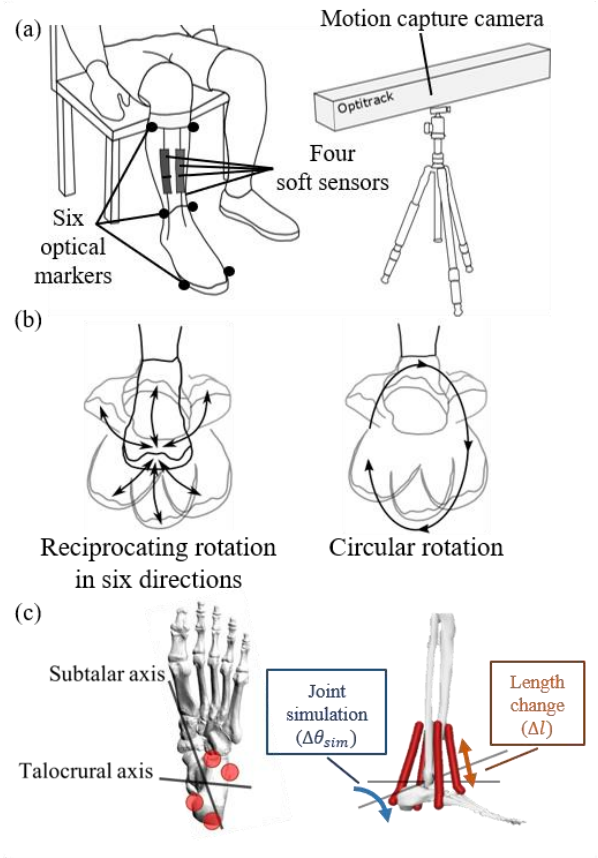

Fig. 5: Experimental setup: (a) measurement of ankle movements using the proposed brace and a motion capture system; (b) movement protocols in the motion capture experiment, i.e., reciprocating rotation in six directions and circular rotation; (c) musculoskeletal model, including the axes of rotation and the four virtual muscles, in OpenSim.

OpenSim 4.0 software [29], which has been widely used for simulation-based approaches to wearable robotics [32], [33]. The lower-limb model 2010 of Stanford University was used [34]. The skeleton in this model has predetermined joint axes and the dimensions of the bones are based on a 170 cm tall male. Virtual muscles were attached at the joint in accordance with the locations and orientations of the four strain sensors, as shown in Fig. 5(c). Both ends of the virtual muscles were fixed to the bone in accordance with the geometry of the wires and Velcro cuff. Since the simulation is using a forward-kinematics-based approach, stiffness and damping were not considered. We extracted the relationship between the change in the virtual muscle length (Δl) and the change in the ankle angle ($\Delta\theta_{sim}$). The ROM for two-DOF ankle motions was set to -40° (plantar flexion) to 20° (dorsiflexion) for the talocrural joint axis and -20° (supination) to 30° (pronation) for the subtalar joint axis. This ROM was discretized, and simulations were performed for a total of 806 combinations of the two rotational angles (31 cases of the talocrural angle and 26 cases of the subtalar angle).

C. Neural Network Architecture

The network architecture developed for transfer-learning -based calibration consists of three parts, namely, a sensor

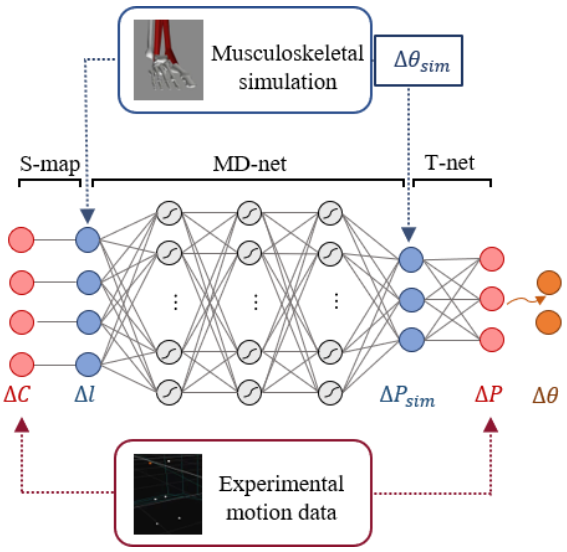

Fig. 6: Schematic of the proposed transfer-learning-based calibration model [S-map, sensor calibration map; MD-net, motion-decoding network; T-net, transfer network; ΔC, measured sensor capacitance; Δl, deformation length; ΔP, coordinates of the center of the foot in Cartesian coordinates defined with respect to the ankle joint; Δθ, ankle joint angle; sim, quantity estimated through simulation].

calibration map (S-map), a motion-decoding network (MD-net), and a transfer network (T-net), as shown in Fig. 6. Because of the significant reduction in hysteresis enabled by the hardware design, the neural network architecture is designed with a time-invariant structure instead of a time-series-oriented architecture, such as a recurrent neural network (RNN) or LSTM architecture. Therefore, our calibration design relies on a simple model structure with low data needs, thus enabling fast training.

The S-map has a simple linear structure with a diagonal matrix that maps the sensor signal (ΔC) to the sensor deformation (Δl) on the basis of experimentally verified calibration gradients, as shown in Fig. 2(b); this part of the architecture does not need to be trained, which is why we call it a 'map'. The MD-net solves for the inverse model of the musculoskeletal simulation $(\Delta l \rightarrow \Delta\theta_{sim} \rightarrow \Delta P_{sim})$; this network is designed with three fully connected hidden layers with a *tanh* activation function. The number of common neurons is empirically set to 16. The T-net's role is the fine-tuning of the simulated results (ΔP_{sim}) by considering the actual motion results (ΔP) for an individual.

While the ultimate objective of calibration is to monitor the joint angles, we initially map the sensor signals to the relative coordinates of the foot with respect to a Cartesian coordinate system that is defined such that the x-y plane contains the two ankle joint axes (talocrural and subtalar) and their center, representing the center of the ankle joint. The reason is that matching the angle differences between the simulation and the real measurements would require a nonlinear relationship, whereas these Cartesian coordinates can be matched with a linear relationship. The x axis was set as same direction with talocrural joint axis and y axis was virtually generated by extracting the basis vector from the

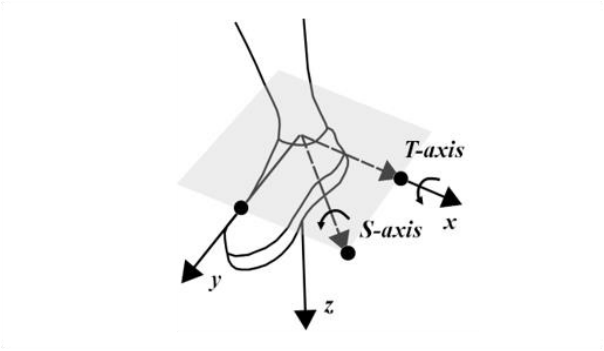

Fig. 7: Coordinates used for data representation.

subtalar joint, as shown in Fig. 7. Based on observations, we designed the T-net with a linear mapping to enable easy and fast regression based on a small dataset, thereby enabling fast and computationally efficient calibration. After estimation of the Cartesian foot coordinates, the Cartesian result ΔP is then transformed into the joint angle ($\Delta\theta$). For comparison with the proposed transfer-learning-based calibration model (*transfer model*), we also trained a direct end-to-end calibration model (*direct model*) with exactly the same neural network architecture as that of the transfer model.

D. Training

The first step of training the transfer model is to train the MD-net on a simulation dataset. We conducted this training process using a mean squared error (MSE) loss function and the adaptive moment estimation (ADAM) optimizer with a learning rate of 0.0005 [35]. The next stage of training is to fine-tune the model by training the T-net on an actual motion capture dataset; for this purpose, the MSE loss function and the ADAM optimizer with a learning rate of 0.0001 were used. Various methods of linear regression are available; in this study, we used the iterative gradient descent method to ensure fair quantitative comparisons. For the direct model, we also used the MSE loss function and the ADAM optimizer, and we set the learning rate to 0.0001. The mini-batch size was set to approximately 1% of the number of training samples, and overfitting during training was prevented by using the conventional method of dividing the dataset into training, validation, and test sets (at a ratio of 8:1:1). To show that the proposed calibration model can be constructed using fewer data, we used only part of the training dataset to train this model. The same validation dataset was used for both models. All of the results discussed in the next section are inferences obtained by applying the trained models to the test dataset. The training processes were conducted with Keras (TensorFlow) backend and a single 11 GB NVIDIA GeForce GTX 1080 Ti GPU.

IV. Results

To validate the performance of the proposed transfer -learning-based calibration method, we quantitatively evaluated its motion measurement accuracy, the generalizability of its measurement performance, and the computational cost of training the model. Referring the fact that data-driven approaches exhibit superior performance than linear approaches [7], [18], we took experiments only with data-driven calibration models.

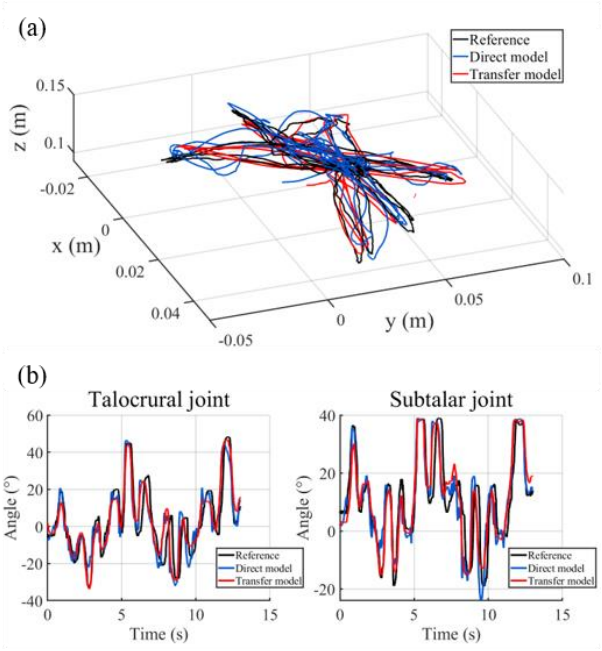

Fig. 8: Estimated trajectories of ankle movements during reciprocating rotation in six directions based on (a) x-y-z Cartesian coordinates and (b) the angle values corresponding to the two ankle joint axes.

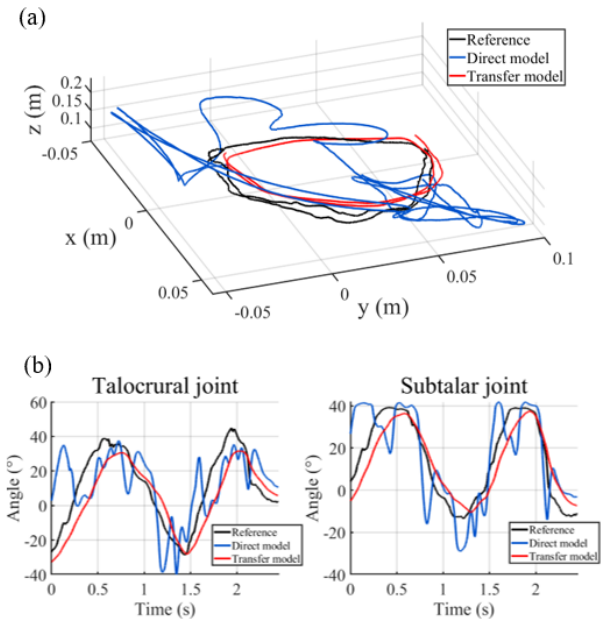

Fig. 9: Estimated trajectories of ankle movements during circular rotation based on (a) x-y-z Cartesian coordinates and (b) the angle values corresponding to the two ankle joint axes.

A. Accuracy of Predefined Motion Measurement

For a given predefined motion, the monitoring performance depends on the capabilities of the model itself [7], [20], [27]. In this work, we analyzed the accuracy of estimating reciprocating rotation in six directions, the session 1 motion, described in section III-A. The accuracy of a motion measurement is represented by the *tracking error*, calculated as the root-mean-square error (RMSE) between the angle estimated by the model and the actual angle measured. To visualize the joint motion trajectories, we monitored the changes in the joint angles and transformed the trends of the joint angles into Cartesian coordinates. The visualized trajectories provide an intuitive view of the joint motion trends as a supplement to the RMSE values.

The definition of the coordinate system is illustrated in Fig. 7. The visualized trajectories and the estimated joint angles show that both models are capable of tracking movements in all six directions with sufficient performance, as shown in Fig. 8. Values that lie outside the ROM of each individual rotational axis are not misrepresented; they are the result of simultaneous rotation around both the talocrural and subtalar joint axes, as these axes are non-orthogonal and thus exhibit interdependency. The results are not overfitted to the data, as discussed in section III-D. A quantitative evaluation shows that the difference between the models corresponds to an average tracking error of only 1.33° and a maximum error of 2.43°, as shown in Table 1. The direct model achieves a slightly better tracking error than the proposed transfer model does. However, because the deep learning process is a non-convex optimization problem, there is no guarantee that the current result is globally optimal. Therefore, a quantitative comparison of the exact RMSE values may not be meaningful. Nevertheless, the comparable RMSE levels indirectly suggest

Table I: Tracking errors for six-directional motions and circular motions at the ankle [RMSE, root-mean-square error in degrees].

	Six directions (RMSE)		Circular motion (RMSE)	
	Direct model	**Transfer model (proposed)**	**Direct model**	**Transfer model (proposed)**
S1	4.44	5.22	21.6	10.8
S2	4.89	6.34	9.16	6.54
S3	5.09	5.97	11.3	8.88
S4	4.75	7.18	21.0	15.0
S5	4.59	5.70	26.3	18.9

that the proposed transfer-learning-based calibration method is able to achieve a level of performance close to that of the direct model while having an advantage in terms of utilization because of the extremely simple linear transformation used in the calibration step.

B. Generalized performance to Arbitrary Motions

Generalizability refers to the capability of a model to estimate arbitrary output that is not considered during the training process. There is no standardized method of quantitatively validating generalizability because it is strongly related to the distribution or domain type of the input dataset, and it is difficult to formulate a method of handling every possible relationship. Therefore, we performed a relative comparison of generalized performance by comparing the tracking errors for a type of joint motion different from the motion used for training. Specifically, we used the same direct model and transfer model mentioned in section IV-A and tested them on circular rotational motions. The results show that the proposed transfer model exhibits superior generalizability of estimation performance, with an average

Table II: Comparisons of computational cost for the proposed method using transfer model and the direct model.

	Sample size	Time per epoch (ms)	Total epoch
Direct model	18422	1010	1986
Transfer Model (proposed)	620	0.562	2143

tracking error difference of 5.85° and a maximum of 10.8° (Table I). Additionally, the visualized trajectories show higher measurement accuracy and follow the input more closely. The transfer model produces a smooth circular trajectory, while the direct model produces unwanted movements, as shown in Fig. 9. One reason for this higher performance is that the transfer model was trained in advance with all possible joint angle states via simulation. By contrast, it is not practical to measure all possible joint angle states for each user in a motion capture experiment, and even if such measurements could be performed, training a new calibration model from scratch for each individual user would incur a high computational cost.

C. Comparison of Computational Cost

Generally, computational cost can be compared in terms of the model capacity, the sample size of the training dataset, and the computation time. For one subject (S1), the size of the training dataset was set to 18,422 for the direct end-to-end model, and 620 data values were used (see section III-D). With regard to computation time, we measured the training time for each epoch and tallied the total number of training epochs. The results show that the proposed transfer-learning-based model took 1.01 s per epoch and required a total of 1986 epochs to complete the training process. In contrast, the direct end-to-end calibration model took 0.562 ms per epoch and required a total of 2143 epochs (Table II). The result shows significantly improved computation speed with smaller amount of data, while simultaneously achieving improved model performance.

D. Demonstration

We built a real-time sensing brace operation platform based on LABVIEW (National Instruments™, USA). The demonstration platform, as shown in Fig. 10, provides monitoring of the ankle joint angles and the Cartesian coordinates of the center of the foot in the Cartesian plane, as shown in Fig. 6 (see the demonstration video). The operating frequency of the system is set to 250 Hz. The demonstration scenario shows the monitoring of various free movements of the ankle joint, and provides applicability to leisure activity, with dancing scenario.

V. Conclusion

We proposed a soft-sensor-based wearable sensing brace design that improves the accuracy and repeatability of soft sensor measurements as well as a calibration method based on musculoskeletal simulations and transfer learning for improved computational efficiency. We proposed a sensing brace with a novel wire-driven design that ensures that only stretch stimuli are imposed on the strain sensors, thus eliminating unwanted disturbances and reducing the

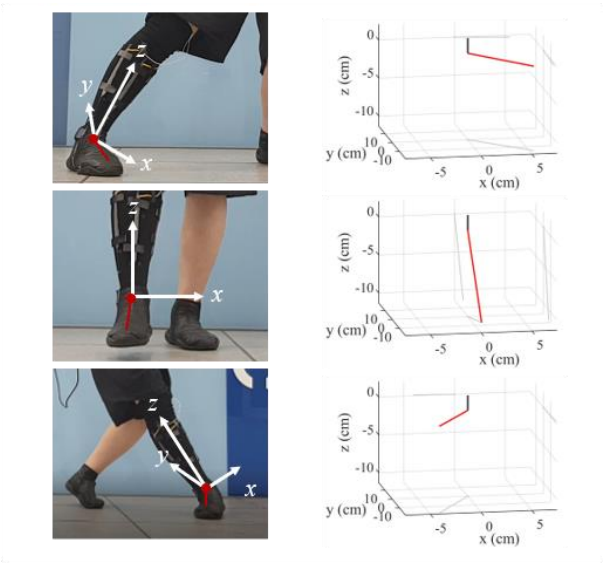

Fig. 10: Scheme of demonstration in dancing scenario.

time-varying property of the response. Additional advantages include high repeatability due to the predefined wire alignment and easy wearability due to the flexible design. We simulated the behavior of multi-DOF ankle joint movements to serve as the basis of a data-driven calibration model. The model was then fine-tuned on measured motion data by means of a simple linear transformation. As a result, our calibration process is fast and computationally efficient and results in model performance comparable to that achieved with the direct end-to-end calibration process. Our approach shows high generalizability for various types of measurements, meaning that a transfer-learning-based model trained on only certain types of measured motion information can be used to monitor arbitrary motions with sufficient measurement performance.

Nevertheless, our approach still has some limitations to be solved. In the current sensing brace design, the length of the strain sensors themselves is too long due to their low stretchability. In addition, the sensors are susceptible to vibration because they are suspended on wires. The improved estimation accuracy can be achieved based on the consideration of dynamic behavior at the sensor calibration network to monitor fast joint motions.

References

[1] H. Zhou and H. Hu, "Human motion tracking for rehabilitation—A survey," Biomed. Signal Process. Control, vol. 3, no. 1, pp. 1–18, Jan. 2008.

[2] G. Ligorio and A. M. Sabatini, "A Novel Kalman Filter for Human Motion Tracking With an Inertial-Based Dynamic Inclinometer," IEEE Trans. Biomed. Eng., vol. 62, no. 8, pp. 2033–2043, Aug. 2015.

[3] R. Lun and W. Zhao, "A Survey of Applications and Human Motion Recognition with Microsoft Kinect," Int. J. Pattern Recognit. Artif. Intell., vol. 29, no. 05, p. 1555008, Aug. 2015.

[4] D. Roetenberg, H. Luinge, and P. Slycke, "Xsens MVN: full 6DOF human motion tracking using miniature inertial sensors," Xsens Motion Technol. BV, …, no. February, pp. 1–7, 2009.

[5] Y. Guo, F. Deligianni, X. Gu, and G.-Z. Yang, "3-D Canonical Pose Estimation and Abnormal Gait Recognition With a Single RGB-D Camera," IEEE Robot. Autom. Lett., vol. 4, no. 4, pp. 3617–3624, Oct. 2019.

[6] J. Fong, H. Rouhani, and M. Tavakoli, "A Therapist-Taught Robotic System for Assistance During Gait Therapy Targeting Foot Drop," IEEE Robot. Autom. Lett., vol. 4, no. 2, pp. 407–413, Apr. 2019.

[7] D. Kim, J. Kwon, S. Han, Y.-L. Park, and S. Jo, "Deep Full-Body Motion Network for a Soft Wearable Motion Sensing Suit," IEEE/ASME Trans. Mechatronics, vol. 24, no. 1, pp. 56–66, Feb. 2019.

[8] Y. Mengüç et al., "Wearable soft sensing suit for human gait measurement," Int. J. Rob. Res., vol. 33, no. 14, pp. 1748–1764, Dec. 2014.

[9] M. Amjadi, K.-U. Kyung, I. Park, and M. Sitti, "Stretchable, Skin-Mountable, and Wearable Strain Sensors and Their Potential Applications: A Review," Adv. Funct. Mater., vol. 26, no. 11, pp. 1678–1698, Mar. 2016.

[10] M. Stoppa and A. Chiolerio, "Wearable Electronics and Smart Textiles: A Critical Review," Sensors, vol. 14, no. 7, pp. 11957–11992, Jul. 2014.

[11] Yong-Lae Park, Bor-Rong Chen, and R. J. Wood, "Design and Fabrication of Soft Artificial Skin Using Embedded Microchannels and Liquid Conductors," IEEE Sens. J., vol. 12, no. 8, pp. 2711–2718, Aug. 2012.

[12] M. Amjadi, Y. J. Yoon, and I. Park, "Ultra-stretchable and skin-mountable strain sensors using carbon nanotubes–Ecoflex nanocomposites," Nanotechnology, vol. 26, no. 37, p. 375501, Sep. 2015.

[13] T. Yamada et al., "A stretchable carbon nanotube strain sensor for human-motion detection," Nat. Nanotechnol., vol. 6, no. 5, pp. 296–301, May 2011.

[14] A. Atalay et al., "Batch Fabrication of Customizable Silicone-Textile Composite Capacitive Strain Sensors for Human Motion Tracking," Adv. Mater. Technol., vol. 2, no. 9, p. 1700136, Sep. 2017.

[15] L. Cai et al., "Super-stretchable, Transparent Carbon Nanotube-Based Capacitive Strain Sensors for Human Motion Detection," Sci. Rep., vol. 3, no. 1, p. 3048, Nov. 2013.

[16] D. Gamby and L. Blugeon, "On the characterization by Schapery's model of non-linear Viscoelastic materials," Polym. Test., vol. 7, no. 2, pp. 137–147, Jan. 1987.

[17] J. C. Case, E. L. White, and R. K. Kramer, "Soft Material Characterization for Robotic Applications," Soft Robot., vol. 2, no. 2, pp. 80–87, Jun. 2015.

[18] D. Kim, M. Kim, J. Kwon, Y.-L. Park, and S. Jo, "Semi-Supervised Gait Generation With Two Microfluidic Soft Sensors," IEEE Robot. Autom. Lett., vol. 4, no. 3, pp. 2501–2507, Jul. 2019.

[19] P. T. Gibbs and H. H. Asada, "Wearable conductive fiber sensors for multi-axis human joint angle measurements," J. Neuroeng. Rehabil., vol. 2, pp. 1–18, 2005.

[20] M. Totaro et al., "Soft Smart Garments for Lower Limb Joint Position Analysis," Sensors, vol. 17, no. 10, p. 2314, Oct. 2017.

[21] H. Lee, H. Cho, S. J. Kim, Y. Kim, and J. Kim, "Dispenser printing of piezo-resistive nanocomposite on woven elastic fabric and hysteresis compensation for skin-mountable stretch sensing," Smart Mater. Struct., vol. 27, no. 2, p. 025017, Feb. 2018.

[22] X. Li, R. Wen, Z. Shen, Z. Wang, K. D. K. Luk, and Y. Hu, "A Wearable Detector for Simultaneous Finger Joint Motion Measurement," IEEE Trans. Biomed. Circuits Syst., vol. 12, no. 3, pp. 644–654, Jun. 2018.

[23] L. Li, S. Jiang, P. B. Shull, and G. Gu, "SkinGest: artificial skin for gesture recognition via filmy stretchable strain sensors," Adv. Robot., vol. 32, no. 21, pp. 1112–1121, Nov. 2018.

[24] S. Han, T. Kim, D. Kim, Y.-L. Park, and S. Jo, "Use of Deep Learning for Characterization of Microfluidic Soft Sensors," IEEE Robot. Autom. Lett., vol. 3, no. 2, pp. 873–880, Apr. 2018.

[25] T. G. Thuruthel, B. Shih, C. Laschi, and M. T. Tolley, "Soft robot perception using embedded soft sensors and recurrent neural networks," Sci. Robot., vol. 4, no. 26, p. eaav1488, Jan. 2019.

[26] M. Gholami, A. Ejupi, A. Rezaei, A. Ferrone, and C. Menon, "Estimation of Knee Joint Angle Using a Fabric-Based Strain Sensor and Machine Learning: A Preliminary Investigation," in 2018 7th IEEE International Conference on Biomedical Robotics and Biomechatronics (Biorob), 2018, pp. 589–594.

[27] S. Dey, M. Eslamy, T. Yoshida, M. Ernst, T. Schmalz, and A. Schilling, "A Support Vector Regression Approach for Continuous Prediction of Ankle Angle and Moment During Walking: An Implication for Developing a Control Strategy for Active Ankle Prostheses," in 2019 IEEE 16th International Conference on Rehabilitation Robotics (ICORR), 2019, pp. 727–733.

[28] K. Weiss, T. M. Khoshgoftaar, and D. Wang, "A survey of transfer learning," J. Big Data, vol. 3, no. 1, p. 9, Dec. 2016.

[29] S. L. Delp et al., "OpenSim: Open-Source Software to Create and Analyze Dynamic Simulations of Movement," IEEE Trans. Biomed. Eng., vol. 54, no. 11, pp. 1940–1950, Nov. 2007.

[30] E. L. White, M. C. Yuen, J. C. Case, and R. K. Kramer, "Low-Cost, Facile, and Scalable Manufacturing of Capacitive Sensors for Soft Systems," Adv. Mater. Technol., vol. 2, no. 9, p. 1700072, Sep. 2017.

[31] H. Zwipp and T. Randt, "Ankle joint biomechanics," Foot Ankle Surg., vol. 1, no. 1, pp. 21–27, Apr. 1994.

[32] R. J. Varghese, X. Guo, D. Freer, J. Liu, and G.-Z. Yang, "A Simulation-based Feasibility Study of a Proprioception-inspired Sensing Framework for a Multi-DoF Shoulder Exosuit," in 2019 IEEE 16th International Conference on Wearable and Implantable Body Sensor Networks (BSN), 2019, pp. 1–4.

[33] Y.-L. Park et al., "Design and control of a bio-inspired soft wearable robotic device for ankle–foot rehabilitation," Bioinspir. Biomim., vol. 9, no. 1, p. 016007, Jan. 2014.

[34] E. M. Arnold, S. R. Ward, R. L. Lieber, and S. L. Delp, "A Model of the Lower Limb for Analysis of Human Movement," Ann. Biomed. Eng., vol. 38, no. 2, pp. 269–279, Feb. 2010.

[35] D. P. Kingma and J. L. Ba, "Adam: A Method for Stochastic Optimization," in Proc. Int. Conf. Learn. Represent., 2015, pp. 1–41.